Sequential Spatial Transformer Networks for Salient Object Classification

David Dembinsky*[1,2], Fatemeh Azimi*[1,2], Federico Raue[2], Jörn Hees[2], Sebastian Palacio[2], and Andreas Dengel[1,2]

[1]*TU Kaiserslautern, Germany*

[2]*German Research Center for Artificial Intelligence (DFKI), Germany*

{firstname.lastname}@dfki.de

Keywords: Sequential Spatial Transformer Networks, Reinforcement Learning, Object Classification.

Abstract: The standard classification architectures are designed and trained for obtaining impressive performance on dedicated image classification datasets, which usually contain images with a single object located at the image center. However, their accuracy drops when this assumption is violated, e.g., if the target object is cluttered with background noise or if it is not centered. In this paper, we study salient object classification: a more realistic scenario where there are multiple object instances in the scene, and we are interested in classifying the image based on the label corresponding to the most salient object. Inspired by previous works on Reinforcement Learning and Spatial Transformer Networks, we propose a model equipped with a trainable focus mechanism, which improves classification accuracy. Our experiments on the PASCAL VOC dataset show that the method is capable of increasing the intersection-ver-union of the salient object, which improves the classification accuracy by 1.82 pp overall, and 3.63 pp for smaller objects. We provide an analysis of the failing cases, discussing different aspects such as dataset bias and saliency definition on the classification output.

1 INTRODUCTION

With the advancement of deep learning techniques during the last decade (Krizhevsky et al., 2012; Vaswani et al., 2017), these methods achieve impressive performance in a variety of tasks such as image classification and object detection (He et al., 2015; Ren et al., 2015). The majority of architectural advances based on Convolutional Networks (Xie et al., 2017; Szegedy et al., 2017) or Transformer Networks (Dosovitskiy et al., 2020) evaluate on high-quality data such as CIFAR (Krizhevsky et al., 2009) or Imagenet (Deng et al., 2009). However, a side-product of focusing on increasing the model accuracy on specialized and curated datasets is the lack of out-of-domain generalization (Hendrycks and Dietterich, 2019) and poor performance on images where the region of interest (RoI) is not placed in the center of the image, let alone if the scene is cluttered (Jaderberg et al., 2015; Azimi et al., 2019).

In this paper, we study the task of salient object classification: A setup in which we aim at classifying the most salient object in a scene where there are multiple object instances. Previous work has proposed various solutions for this task including attention by (Mnih et al., 2014) or employing spatial transformer networks (STN), transforming the input such that it is easier to classify (Jaderberg et al., 2015; Azimi et al., 2019); however, these methods were mainly applied to simplistic scenarios and synthetic datasets.

In this work, we build on top of the Sequential Spatial Transformer Network (SSTN) algorithm (Azimi et al., 2019). We extend their work by multiple architectural and design improvements and evaluate our model on the challenging real-world dataset PASCAL VOC (Everingham et al., 2010). We choose this method as the RL-based solution in (Azimi et al., 2019) allows us to employ a variety of non-differentiable training objectives.

Our main hypothesis is that zooming in on the salient object and cropping out secondary objects regarded as clutter is beneficial for the classifier. Hence, increasing the Intersection over Union (IoU) of the salient object (i.e. the ratio between the salient object's bounding-box area and the image area) can be used as a training signal. We study this assumption in Section 4.3.1.

Thanks to the availability of object detection

[*] Equal contribution

information in PASCAL VOC (Everingham et al., 2010), we use bounding-box information to compute the IoU of different object instances in the scene. Instead of relying on human annotations for identifying the salient object, we resort to the following approximation: we assume object size as an estimator for saliency and consider the largest object as the salient one. We extend the algorithm proposed in (Azimi et al., 2019) by employing Q-Learning, which is a more effective algorithm in terms of scaling to high dimensional input data such as images. Moreover, we propose reward-shaping functions that attempt to directly increase the IoU of the salient object, resulting in improved classification accuracy. Our method named DQ-SSTN increases the IoU of the salient object by 11.31 pp and the overall classification accuracy by 1.82 pp. We observe that our method is especially effective for smaller objects (objects that cover less than 20 percent of the image area), where we obtain an improvement of 3.63 pp in accuracy. In Section 4.4 we study the effect of the dataset characteristics and saliency assumptions in failure scenarios.

2 RELATED WORK AND BACKGROUND

In this section, we provide the preliminaries used as the foundation of our work. We briefly give an overview of the utilized algorithms from the reinforcement learning literature, followed by an introduction to Sequential Spatial Transformer Networks.

2.1 Reinforcement Learning

Reinforcement Learning (RL) is a learning paradigm for training a learner (agent) by maximizing an objective via interacting with an environment and learning from the acquired experiences (Sutton and Barto, 2018). The RL framework is based on a Markov Decision Process (MDP) consisting of a set of states s, actions a, and rewards r. The goal is to train an agent which maximizes the reward function via searching for the optimal action-selection policy through interactions with the environment, as shown in Figure 1. Each action selection results in receiving a reward and a change in the current state.

The proposed algorithms for finding the optimal action policy can be categorized into two main groups of Policy Gradient and Q-learning. In this paper, we utilize Q-learning due to its good performance in processing high-dimensional states such as images (Mnih et al., 2013). In Q-learning, the model learns a value function q^* that estimates the expected reward for each state-action pair. This function is learned based on the Bellman Optimality equation:

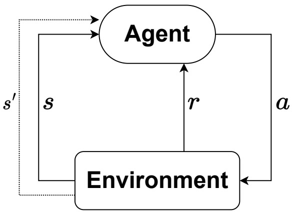

Figure 1: The episodic MDP: First the agent observes the environment's state s and selects an action a which changes the state to s'. Based on the impact of the action, the agent receives the reward r. We train the agent to choose a sequence of actions leading to the maximum expected reward.

$$q^*_\theta(s,a) = r(s,a) + \gamma \max_{a'} q^*_\theta(s'(s,a),a') \qquad (1)$$

where γ is a hyperparameter and θ represents the network's parameters. Since Equation 1 is greedy (max operator) and initially the model is not trained, we use the ε-greedy strategy, a trade-off between exploration of the state-action space and exploitation of the expected rewards (Equation 2). Exploration decreases with the number of taken steps n with decay d:

$$a = \begin{cases} a_{\text{rand}}, & \text{if } p < \varepsilon_{\text{end}} + (1-\varepsilon_{\text{end}}) \cdot e^{-\frac{n}{d}} \\ \arg\max_{\hat{a}} \; q^*(s,\hat{a}), & \text{otherwise} \end{cases} \qquad (2)$$

a_{rand} corresponds to an action selected randomly, $p \sim U(0,1)$, and ε_{end} and d are hyperparameters.

In Equation 1, there is a strong correlation between consecutive updates, which is detrimental to the training procedure. This limitation is addressed by utilizing a replay memory (Mnih et al., 2013), as a way to break the correlation between the training samples. In the replay memory, each experience (s,a,r,s') is stored in a buffer and then drawn at random to perform a training step. Since the update rule in Equation 1 is dependent on the old parameters itself (θ), a target network is additionally used for predicting the expected reward (Mnih et al., 2015). The target network has an identical architecture as the agent network (q in Equation 1). It is not trained by gradient descent, but its weights are periodically updated from the agent network.

2.2 Spatial Transformer Networks

The Spatial Transformer Network (STN) (Jaderberg et al., 2015) is a network architecture proposed to learn modifying the input image by generating parameters of an affine transformation. The network's parameters are trained by minimizing a differentiable

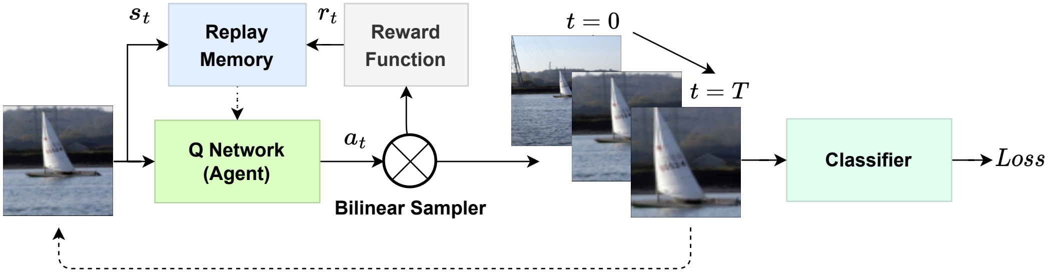

Figure 2: The overall architecture of DQ-SSTN. Our model sequentially modifies the input image by applying a series of simple and discrete transformations (a_t) selected by an agent trained to maximize the overall obtained reward (r_t).

objective such as classification loss. (Azimi et al., 2019) propose a Sequential Spatial Transformer Network (SSTN), which uses RL to find the optimal transformation. Rather than generating continuous transformation parameters, they decompose the transformation into a sequence of discrete and predefined simple transformations, which are chosen iteratively.

We extend their approach, as the RL-based formulation allows us to work with non-differentiable objectives, as discussed in the following section.

3 METHOD

In this section, we study the problem of salient object classification where saliency is determined based on an object's bounding-box size, as discussed further in Section 4.1.1 Opposite to standard image classification models working with curated images centered around a single salient object (Krizhevsky et al., 2009; Deng et al., 2009), we focus on a more realistic scenario where input images are cluttered with multiple objects and the network has to classify the image based on the most salient object. Since the original SSTN method (Azimi et al., 2019) is limited to processing small, gray-scale images, our goal is to extend this algorithm for working with real-world data.

While SSTN uses Policy Gradient for training the RL agent, we employ the Q-learning algorithm as it works better for higher-dimensional data. Additionally, we experiment with a variety of reward functions, that based on different metrics, aim to boost the performance of the downstream classifier. Thanks to the RL-based framework, our model is flexible to work with non-differentiable training objectives. Figure 2 visualizes the overall architecture of our model.

As mentioned in Section 2.1, to describe the MDP framework, we have to define state space, action set, and reward functions. For the **state space** s_t, we consider the transformed image at time t which has undergone a sequence of transformations (the actions selected by the agent). Our **action set** a_t consists of 6 discrete affine transformations with fixed parameters including translation in 4 directions, zooming and *identity*. *Identity* allows early stopping while training in batches and using a fixed transformation length T.

Regarding the **reward** r_t, we initially experiment with the functions proposed by (Azimi et al., 2019) referred to as *Continuous loss-reward* and *Discrete Acc-reward*. *Continuous loss-reward* is the difference between the classification loss before and after applying the selected action (hence the reward is positive when reducing the loss value). *Discrete Acc-reward* rewards the agent with $+1$ if the classifier's prediction changes from incorrect to correct or -1 vice-versa.

We further explore the possibility of improving the classifier accuracy by learning to increase the IoU of the salient object. To this end, we positively reward the agent when the selected action results in increasing the area of the salient object. This way, the agent is encouraged to zoom around the salient object. This reward named *Continuous IoU-reward* is defined as:

$$r_t^{(c\_iou)} = \mathrm{IoU}_t - \mathrm{IoU}_{t-1} \tag{3}$$

We also experiment with the discrete version of the IoU and refer to it as *Discrete IoU-reward*:

$$r_t^{(d\_iou)} = \begin{cases} +1, & \text{if } \mathrm{IoU}_t > \mathrm{IoU}_{t-1} \\ -1, & \text{if } \mathrm{IoU}_t < \mathrm{IoU}_{t-1} \\ 0, & \text{else} \end{cases} \tag{4}$$

The last reward for training the model is a weighted combination of loss-reward and IoU-reward, using hyperparameters α and β:

$$r_t^{(combined)} = \alpha \cdot r_t^{(c\_loss)} + \beta \cdot r_t^{(d\_iou)} \tag{5}$$

The objective for training the classifier is the standard cross-entropy loss, and for the DQ-SSTN we use Huber loss, a loss that serves as a compound of absolute and squared loss (Huber, 1964).

4 EXPERIMENTS

In this section, we provide the implementation details, as well as an analysis of the obtained results on the PASCAL VOC dataset (Everingham et al., 2010). The code is publicly available[1].

4.1 Implementation Details

4.1.1 Dataset

For evaluation, we use PASCAL VOC (Everingham et al., 2010), a real-world dataset with pictures containing multiple objects from 20 object classes. The dataset provides the bounding box and the category of each object. We combine the versions of 2007 and 2012 to get as many images as possible, resulting in a training set of 8218 and a test set of 8333 frames.

For the classification ground-truth label, we consider the category of the object with the largest area. Consequently, the *Top-1* accuracy depends on whether the prediction corresponds to the largest visible object. As additional metrics, we use the *Top-2* and *Any* accuracies for evaluation (we only optimize over Top-1 accuracy). The *Top-2* accuracy additionally allows the prediction to be the second largest object, and the *Any* accuracy permits the prediction to match any object present within an image.

We highlight that using the PASCAL VOC dataset for single-class labeling results in a non-uniform class distribution, where class *person* has more than 1700 images compared to other classes, which range from below 200 to 600 images per class. We discuss a possible bias towards the dominant class in Section 4.4.1.

4.1.2 Training Setup

The backbone of the classifier and the Q-network consists of a ResNet18 (He et al., 2015) where the last fully connected layer is modified to match the number of the object classes and the number of actions, respectively. ResNet18 is an architecture quite successful in image classification tasks, and the library PyTorch (Paszke et al., 2017) provides pre-trained weights. We downscale the input images to 224×224 to match the ResNet18s implementation and perform horizontal flipping augmentations to increase the variety in the dataset. We document the best set of hyperparameters found by experimentation. The replay memory stores 1000 transitions. The ε-greedy strategy Equation 2 uses $d = 50000$ and $\varepsilon_{\text{end}} = 0.05$. For Q-Learning (Equation 1) we use $\gamma = 0.95$ and update our target-net after 100 agent updates. We train our model with Adam (Kingma and Ba, 2015) optimizer and a learning rate of $5 \cdot 10^{-6}$ for 50 epochs. The trajectories are constructed with a length of $T = 10$ transformations. The DQ-SSTN's transformations include translation by 4 pixels in each cardinal direction and zooming-in by a factor of 0.8. The weight factors in Equation 5 used are $\alpha = 1$ and $\beta = 0.8$.

4.2 Main Results

Table 1 provides a comparison between the baseline classifier without DQ-SSTN and our proposed DQ-SSTN method using different reward functions. As can be seen from the results, the best accuracy was obtained employing the discrete IoU reward, improving *Top-1* accuracy by 1.82 pp, *Top-2* accuracy by 1.86 pp and *Any* accuracy by 1.23 pp, respectively.

In Figure 3, we provide an analysis of the IoU and classification accuracy using the best-found setup. We visualize the IoU of the target class before and after applying the transformations selected by our DQ-SSTN model. To better understand the impact of the transformations on objects with different sizes, we divide the test-set images into 5 bins, considering the initial IoU. Applying the DQ-SSTN transformations leads to an average increase of 11.31 pp in the target class IoU (the dotted line in this figure shows the average IoU per bin). Additionally, we evaluate the classification accuracy for each bin before and after applying transformations. We observe that our model is more effective in improving the classification accuracy of smaller objects, increasing it by 3.63 pp for objects with an IoU less than 20%. Interestingly, the IoU of the right-most bin decreases while the accuracy increases; this behavior will be observed in Section 4.3.1 again and discussed in Section 4.4.2.

Visual examples of the transformations learned by our model are illustrated in Figure 7.

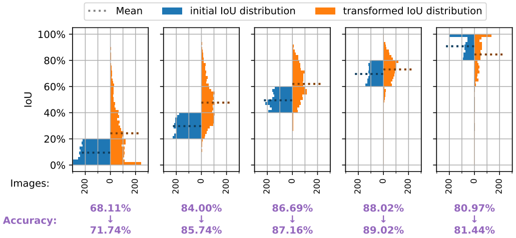

Figure 3: IoU and classification accuracy before and after applying the DQ-SSTN transformations. The dataset is split into five bins according to the initial IoU. Classification accuracy changes are noted under each column. DQ-SSTN is especially useful for smaller objects (first bin) where the classification accuracy is improved by 3.63 pp.

[1] https://git.opendfki.de/david.dembinsky/dq-sstn

Method	**Top-1 (%)**	**Top-2 (%)**	**Any (%)**
Baseline classifier	80.04	82.97	88.22
Continuous loss-reward (r^{c_loss})	80.84	83.75	88.83
Discrete Acc-reward (r^{d_acc})	80.43	83.61	88.67
Continuous IoU-reward (r^{c_iou})	80.15	83.09	88.19
Discrete IoU-reward (r^{d_iou})	**81.86**	**84.83**	**89.45**
Weighted combination-reward ($r^{combined}$)	81.54	84.56	89.27

Table 1: Comparison of classification accuracy of the baseline with our method when using different reward functions, on PASCAL VOC (Everingham et al., 2010). We obtained the best results with the discrete IoU-based reward signal.

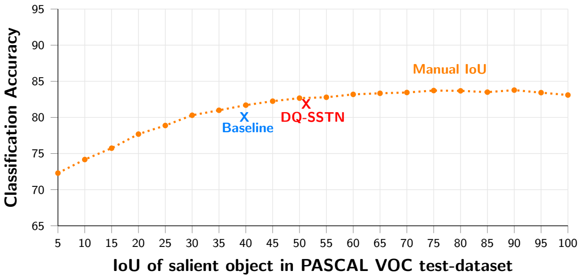

Figure 4: Our experiment indicates a correlation between salient object IoU and classification accuracy (both in %). Zooming on the target object (increase in IoU) leads to better classification accuracy for this object.

4.3 Ablation

4.3.1 Correlation of IoU and Accuracy

The main idea behind our DQ-SSTN is to zoom in on the most salient object. The underlying assumption is that classification accuracy improves with increasing the target object's IoU. To confirm this, we run an experiment where we construct multiple datasets, each with a constant IoU enforced synthetically. To this end, we determine the salient object by the size of the bounding box and crop around it such that we achieve a fixed IoU for that object. Furthermore, we include random translations to hinder the network from cheating and getting biased based on the positioning of the object. This results in a dataset, where each image's salient object has the same, constant IoU.

After constructing 20 datasets with different IoUs, we train and evaluate a classifier on each dataset separately. As can be seen in Figure 4, an increase in the IoU indeed leads to improved classification accuracy. We observe, that adjusting the IoU to more than 90% reduces the accuracy. This shows that extreme zooming has a negative impact on performance, as informative parts of the object can be displaced out of the classifier's focus (Selvaraju et al., 2016; Zhou et al., 2016). We discuss this more in-depth in Section 4.4.2.

4.3.2 Hard mining

Our PASCAL VOC dataset suffers from a considerable imbalance in both class distribution and IoU distribution. This imbalance might hurt performance as the learned solution could be biased towards the dominant category. Hard mining is a training technique that has been proven effective (Shrivastava et al., 2016; Dong et al., 2017) to alleviate the effect of data imbalance by assigning a higher weight to underrepresented (therefore more challenging) data samples.

To this end, we experiment with multiple hard-mining strategies and provide the results in Table 2. As our overall objective consists of the classification and the reward maximization terms, we can perform hard mining by re-weighting the classifier's loss or the reward of the more challenging data samples.

Initially, we consider IoU as a measure of a data sample hardness. Therefore, we reweigh either the loss function or the reward signal by the inverse of IoU, assigning higher importance to samples with smaller IoU (*Weight reward by inverse IoU* and *Weight loss by inverse IoU*). Surprisingly, our results did not improve with this technique. Next, we reweigh the data samples based on the performance of the baseline classifier. If an image is classified incorrectly, we assign a weight of 1 and, if it's predicted correctly, a constant weight < 1. This assigns higher importance to those images which are more difficult for our classifier (*Weight reward by accuracy* and *Weight loss by accuracy*). The results show small improvements of 0.06 pp for either Top-1 or Top-2 accuracy, hence, we do not find these techniques useful to our algorithm.

4.4 Limitations

In this section, we provide a detailed analysis of the results to better understand the impact of the dataset and the assumptions that we made about object size and saliency. We observe that the dominance of class *person* biases the classifier's prediction. Additionally, we show that defining saliency is a non-trivial task and can have a serious impact on the model.

Method	**Top-1 (%)**	**Top-2 (%)**	**Any (%)**
Baseline classifier	80.04	82.97	88.22
DQ-SSTN without hard mining	81.80	85.25	**89.72**
Weight reward by inverse IoU	81.40	85.13	89.60
Weight loss by inverse IoU	81.08	84.72	89.32
Weight reward by accuracy	**81.86**	84.83	89.45
Weight loss by accuracy	81.75	**85.31**	89.69

Table 2: The impact of different hard-minig techniques tried on the classification accuracy. Whilst the *weight by accuracy* methods improved the Top-1 or Top-2 metric, respectively, by 0.06pp, we do not consider this as a noteworthy improvement.

4.4.1 Bias of the Person Class

One property of the PASCAL VOC dataset is an imbalance in the class distribution. Based on object size, about 20% of all images are assigned to *person* class. As a result, we observe that the attention of our DQ-SSTN gets drawn towards persons: If a person is present in the scene, the classifier is biased towards classifying the image as *person* category. In Table 3, we provide statistics for misclassifications considering whether a person is present as a secondary object. It is clearly visible, that in cases where a person is present, the classifier is biased toward this class. However, if there is none the image, the classifier does not overly tend towards predicting one. Note that a random classifier would select *person* class around 20% of the time, following the dataset distribution in the training set. This problem is introduced by the PASCAL VOC dataset, as there are far more person objects throughout the dataset than others.

(%)	**pred.** ***person***	**pred. other**
person present	39.37	60.63
person not present	11.15	88.85

Table 3: The prediction of the classifier on images that were predicted incorrectly. If there is a person present, the DQ-SSTN has a high chance of focusing on it.

4.4.2 Issues with Saliency Assumption

The way we changed the detection dataset into one for classification depends on our saliency assumption: We assume the object with the biggest bounding box to be the most salient one, as described in Section 4.1.1. In this section, we investigate how often and to which extent this assumption is violated and how this impacts the performance of the DQ-SSTN.

An example in contrast with our saliency assumption is when a smaller object is located in front of a bigger one. Consider a person sitting on a sofa (as in Figure 5); in this scenario, humans consider the person as the salient object, while based on our assumption, the sofa is labeled as the salient category. Interestingly, we observed that in most cases the classifier also predicts the front object as the correct class (*person* in this example), but this is considered a misclassification based on our evaluation.

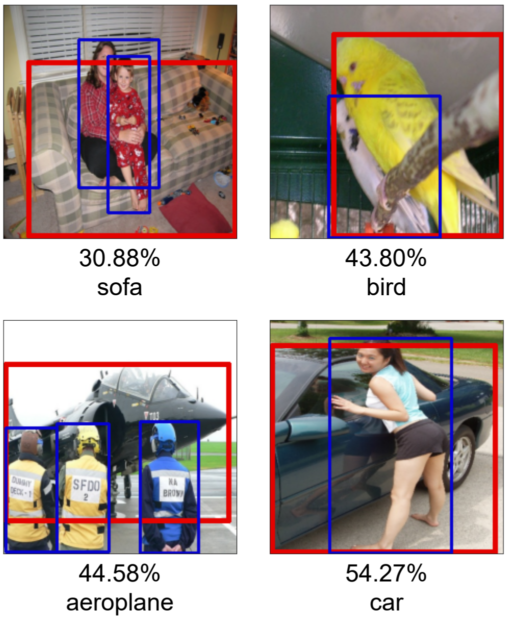

Figure 5: Visual examples where the main object intersects with other objects. Red frames surround the largest object, and blue frames the secondary ones. The value below each image is the percentage of the largest (salient) object's bounding box that intersects with other bounding boxes and the assigned true label is also given. The first image is an image below threshold $th = 0.4$ but still considered cluttered, and the second one is vice versa. The other two examples further highlight our choice of threshold.

To better understand this issue, we visualize the overlap characteristics of our data in Figure 6. In this figure, we see the portion of images in which the main object (largest/salient) is not overlapping with other objects in the scene, as well as the number of images in which the main object intersects with other object instances considering different overlap thresholds. For example, the column with $th = 0.5$ shows the number of images in which the overlap between the main and the secondary objects is lower or higher than 50% of the main object area. We observed that 41.35% of the images only have one object and

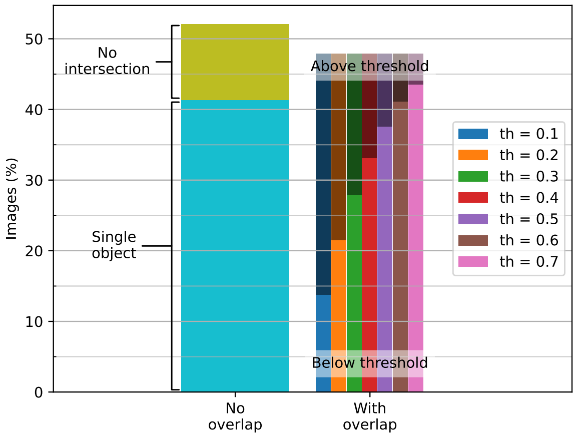

Figure 6: This histogram shows the composition of our dataset regarding the relation between the most salient object and overlapping objects. Depending on the selected threshold, between $5\%(th = 0.7)$ to $35\%(th = 0.1)$ of all images are to some extent covered by another object instance, thus violating our assumption of saliency.

	Accuracy (%)
Total	81.86
No clutter	86.05
Cluttered, below $th = 0.4$	82.83
Cluttered, above $th = 0.4$	64.88

Table 4: DQ-SSTN classification accuracy on each subset of PASCAL VOC when categorized based on the overlap threshold of 0.4 (as shown in Figure 6).

10.76% of all images are accompanied by secondary objects, but their bounding boxes do not intersect with each other. This means that in 52.12% of the images, our assumption about saliency strictly holds. However, in 47.88% of the images, the salient object is to some extent intersecting with (and possibly being occluded by) another object. Looking at some qualitative examples (Figure 5), we consider a threshold of $th = 0.4$ as critical; i.e. all images that have more than 40% of their bounding-box concealed by another object do not follow our saliency assumption based on object size. Based on this threshold, about 15% of the dataset conflict with our saliency assumption.

To investigate the impact of our saliency assumption on the DQ-SSTN performance, we divide the dataset into three categories; the images with the main object not covered by any other objects and the images in which the main object is covered by other instances more *or* less than 40% ($th = 0.4$ in Figure 6) We evaluate our model separately on each group and present the results in Table 4. As expected, we observe that the classification accuracy is significantly lower for the data in which the salient object has an overlap of over 40% with other objects in the scene.

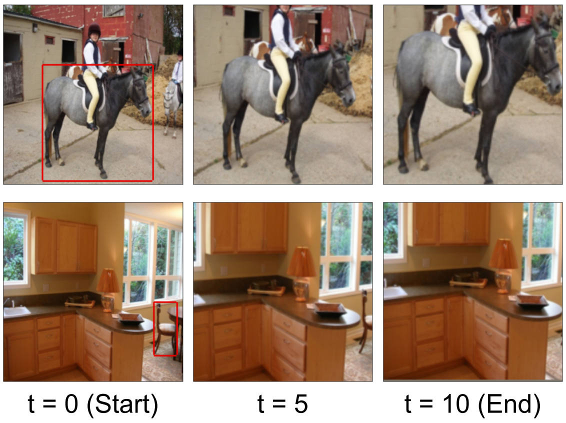

t = 0 (Start) t = 5 t = 10 (End)

Figure 7: Visual examples of our DQ-SSTN model gradually focusing on the salient object. The bounding box of the largest object is visualized in red in the starting frame (t=0). The first row is an example of the DQ-SSTN working as expected. The second row is a failing case, where the DQ-SSTN cannot find the salient object and blindly zooms in.

5 CONCLUSION AND FUTURE WORK

In this paper, we study the task of salient object classification. We introduce DQ-SSTN, a Sequential Spatial Transformer Network based on Deep Q-Learning. Our model learns to zoom on the salient object by iteratively selecting an affine transformation to increase the IoU of the largest object in an image. We experimentally demonstrate the effectiveness of our method in improving the classification accuracy, especially for smaller objects where we achieve an improvement of 3.63 pp. Furthermore, we provide several ablation studies to investigate the reason behind failure scenarios. In future work, we plan to explore more flexible solutions by considering all objects within an image during training favoring a multi-labeling approach where the DQ-SSTN successively classifies every object within the image. Moreover, we believe working towards preparing a more dedicated dataset free from class bias would benefit our work.

Acknowledgment

This work was supported by the TU Kaiserslautern CS PhD scholarship program, the BMBF project ExplAINN (01IS19074), and the NVIDIA AI Lab (NVAIL) program.

REFERENCES

Azimi, F., Raue, F., Hees, J., and Dengel, A. (2019). A reinforcement learning approach for sequential spatial transformer networks. In Tetko, I. V., Kůrková, V., Karpov, P., and Theis, F., editors, *Artificial Neural Networks and Machine Learning – ICANN 2019: Theoretical Neural Computation*, pages 585–597, Cham. Springer International Publishing.

Deng, J., Dong, W., Socher, R., Li, L.-J., Li, K., and Fei-Fei, L. (2009). Imagenet: A large-scale hierarchical image database. In *2009 IEEE conference on computer vision and pattern recognition*, pages 248–255. Ieee.

Dong, Q., Gong, S., and Zhu, X. (2017). Class rectification hard mining for imbalanced deep learning. In *Proceedings of the IEEE International Conference on Computer Vision*, pages 1851–1860.

Dosovitskiy, A., Beyer, L., Kolesnikov, A., Weissenborn, D., Zhai, X., Unterthiner, T., Dehghani, M., Minderer, M., Heigold, G., Gelly, S., Uszkoreit, J., and Houlsby, N. (2020). An image is worth 16x16 words: Transformers for image recognition at scale. *CoRR*, abs/2010.11929.

Everingham, M., Van Gool, L., Williams, C. K., Winn, J., and Zisserman, A. (2010). The pascal visual object classes (voc) challenge. *International journal of computer vision*, 88(2):303–338.

He, K., Zhang, X., Ren, S., and Sun, J. (2015). Deep residual learning for image recognition. *CoRR*, abs/1512.03385.

Hendrycks, D. and Dietterich, T. (2019). Benchmarking neural network robustness to common corruptions and perturbations. In *International Conference on Learning Representations*.

Huber, P. J. (1964). Robust Estimation of a Location Parameter. *The Annals of Mathematical Statistics*, 35(1):73 – 101.

Jaderberg, M., Simonyan, K., Zisserman, A., and Kavukcuoglu, K. (2015). Spatial transformer networks. In Cortes, C., Lawrence, N., Lee, D., Sugiyama, M., and Garnett, R., editors, *Advances in Neural Information Processing Systems*, volume 28. Curran Associates, Inc.

Kingma, D. P. and Ba, J. (2015). Adam: A method for stochastic optimization. In Bengio, Y. and LeCun, Y., editors, *3rd International Conference on Learning Representations, ICLR 2015, San Diego, CA, USA, May 7-9, 2015, Conference Track Proceedings*.

Krizhevsky, A., Hinton, G., et al. (2009). Learning multiple layers of features from tiny images.

Krizhevsky, A., Sutskever, I., and Hinton, G. E. (2012). Imagenet classification with deep convolutional neural networks. In Pereira, F., Burges, C. J. C., Bottou, L., and Weinberger, K. Q., editors, *Advances in Neural Information Processing Systems*, volume 25. Curran Associates, Inc.

Mnih, V., Heess, N., Graves, A., et al. (2014). Recurrent models of visual attention. *Advances in neural information processing systems*, 27.

Mnih, V., Kavukcuoglu, K., Silver, D., Graves, A., Antonoglou, I., Wierstra, D., and Riedmiller, M. A. (2013). Playing atari with deep reinforcement learning. *CoRR*, abs/1312.5602.

Mnih, V., Kavukcuoglu, K., Silver, D., Rusu, A. A., Veness, J., Bellemare, M. G., Graves, A., Riedmiller, M., Fidjeland, A. K., Ostrovski, G., et al. (2015). Human-level control through deep reinforcement learning. *nature*, 518(7540):529–533.

Paszke, A., Gross, S., Chintala, S., Chanan, G., Yang, E., DeVito, Z., Lin, Z., Desmaison, A., Antiga, L., and Lerer, A. (2017). Automatic differentiation in pytorch. In *NIPS-W*.

Ren, S., He, K., Girshick, R., and Sun, J. (2015). Faster r-cnn: Towards real-time object detection with region proposal networks. *Advances in neural information processing systems*, 28.

Selvaraju, R. R., Das, A., Vedantam, R., Cogswell, M., Parikh, D., and Batra, D. (2016). Grad-cam: Why did you say that? *arXiv preprint arXiv:1611.07450*.

Shrivastava, A., Gupta, A., and Girshick, R. (2016). Training region-based object detectors with online hard example mining. In *Proceedings of the IEEE conference on computer vision and pattern recognition*, pages 761–769.

Sutton, R. S. and Barto, A. G. (2018). *Reinforcement learning: An introduction*. MIT press.

Szegedy, C., Ioffe, S., Vanhoucke, V., and Alemi, A. A. (2017). Inception-v4, inception-resnet and the impact of residual connections on learning. In *Thirty-first AAAI conference on artificial intelligence*.

Vaswani, A., Shazeer, N., Parmar, N., Uszkoreit, J., Jones, L., Gomez, A. N., Kaiser, Ł., and Polosukhin, I. (2017). Attention is all you need. *Advances in neural information processing systems*, 30.

Xie, S., Girshick, R., Dollár, P., Tu, Z., and He, K. (2017). Aggregated residual transformations for deep neural networks. In *Proceedings of the IEEE conference on computer vision and pattern recognition*, pages 1492–1500.

Zhou, B., Khosla, A., Lapedriza, A., Oliva, A., and Torralba, A. (2016). Learning deep features for discriminative localization. In *Proceedings of the IEEE conference on computer vision and pattern recognition*, pages 2921–2929.